DTU Library

The diffusion dynamics of PEGylated liposomes in the intact vitreous of the ex vivo porcine eye: A fluorescence correlation spectroscopy and biodistribution study

Eriksen, Anne Zebitz; Brewer, Jonathan; Andresen, Thomas Lars; Urquhart, Andrew

Link back to DTU Orbit

The Diffusion Dynamics Of PEGylated Liposomes In The Intact Vitreous Of The *Ex Vivo* Porcine Eye: A Fluorescence Correlation Spectroscopy And Biodistribution Study

Anne Z Eriksen[a], Jonathan Brewer[b], Thomas L Andresen[a], Andrew J Urquhart[a]*

[a]Department for Micro- and Nanotechnology, Technical University of Denmark, Building 345C, 2800 Kgs. Lyngby, Denmark

[b]Department of Biochemistry and Molecular Biology, University of Southern Denmark, Campusvej 55, 5230 Odense M, Denmark

*Corresponding author: Andrew J Urquhart (anur@nanotech.dtu.dk)

Abstract

The diffusion dynamics of nanocarriers in the vitreous and the influence of nanocarrier physicochemical properties on these dynamics is an important aspect of the efficacy of intravitreal administered nanomedicines for the treatment of posterior segment eye diseases. Here we use fluorescence correlation spectroscopy (FCS) to determine liposome diffusion coefficients in the intact vitreous (D_{Vit}) of *ex vivo* porcine eyes using a modified Miyake-Apple technique to minimize the disruption of the vitreous fine structure. We chose to investigate whether the zeta potential of polyethylene glycol functionalized (i.e. PEGylated) liposomes altered liposome in situ diffusion dynamics in the vitreous. Non-PEGylated cationic nanocarriers have previously shown little to no diffusion in the vitreous, whilst neutral and anionic have shown diffusion. The liposomes investigated had diameters below 150 nm and zeta potentials ranging from -20 to +12 mV. We observed that PEGylated cationic liposomes

had significantly lower D_{Vit} values (1.14 $\mu m^2 s^{-1}$) than PEGylated neutral and anionic liposomes (2.78 and 2.87 $\mu m^2 s^{-1}$). However, PEGylated cationic liposomes had a similar biodistribution profile across the vitreous to the other systems. These results show that PEGylated cationic liposomes with limited cationic charge can diffuse across the vitreous and indicate that the vitreous as a barrier to nanocarriers (Ø < 500 nm) is more complicated than simply an electrostatic barrier as previously suggested.

1. Introduction

Nanomedicines have been proposed as one of a number of next generation clinical therapies for the treatment of posterior segment eye diseases (Bochot and Fattal, 2012; Liu et al., 2012; del Pozo-Rodríguez et al., 2013). Posterior segment eye diseases - such as diabetic retinopathy and age-related macular degeneration - are vision threatening, remain challenging to treat and increasingly affect a larger proportion of the populations of industrial nations due to increased life expectancy, poor lifestyle and diet (Congdon et al., 2003; Yau et al., 2015). To access the posterior segment of the eye and bypass ocular physiological barriers, nanomedicines are often injected into the vitreous (Geng et al., 2014; Li et al., 2016; Peeters et al., 2005; Zhao et al., 2017; Giannaccini et al., 2014; Natarajan et al., 2014; Sakurai et al., 2001; Thakur et al., 2014). The vitreous fills the vitreous cavity of the eye and has a number of physiological roles (e.g. the regulation of oxygen tension, buffering metabolite diffusion etc. (Foulds, 1987; Holekamp, 2010; Holekamp et al., 2005; Sebag, 2009; Stefansson and Loftsson, 2006)). The vitreous is a hydrogel comprised predominantly of water in a collagen-glycosaminoglygan network (CGN). The CGN comprises of collagen fibres (mainly type II fibrils packed in parallel) separated by random coil glycosaminoglycans (predominantly hyaluronic acid). The density of the CGN varies across the eye with fibrils and fibres predominantly orientating antero-posterior (from lens to retina) (Foulds, 1987; Le Goff and Bishop, 2008; Kodama et al., 2013; Mains and Wilson, 2013; Scott, 1992).

The vitreous has previously been shown to be a barrier to nanocarriers, with the size and surface charge of nanocarriers being argued as crucial factors as to whether nanocarriers can diffuse or are immobilized. The CGN is porous (pores are sometimes described as liquid channels) with porosity changing with CGN density throughout the eye. In the central vitreous, a region of low CGN density, pore size has been shown to vary from 500 nm to over 1 μm (Xu et al., 2013). However, nanocarriers with dimensions greater than 500 nm have been shown to exhibit slow or limited diffusion from injection sites (Xu et al., 2013). This has been attributed to either a limited mobility or immobility through CGN pores. Additionally the CGN is viewed as having a net negative charge due to the large negative charge of glycosaminoglycans   (Mains and Wilson, 2013). Nanocarriers with high cationic zeta potentials ($\geq$ +20 mV) but with diameters below 500 nm have shown limited to no diffusion from the injection site   (Xu et al., 2013). This has been attributed to strong attractive electrostatic interactions with the CGN. Conversely both anionic and neutral nanocarriers have been reported to readily diffuse throughout the vitreous. This has lead to the notion of the vitreous as an electrostatic barrier to nanocarriers (Mains and Wilson, 2013).

The functionalization of nanocarrier surfaces with polyethylene glycol (i.e. PEGylation) has been shown to improve circulation/residency time of nanocarriers and is widely used in nanomedicines. Previous studies have shown that PEGylated neutral polymeric nanoparticles diffuse in the central vitreous with similar values to anionic polymeric nanoparticles (D_{Buffer}/D_{Vit} =1.5-3.2 and 2.2-3.5 respectively) (Martens et al., 2013; Xu et al., 2013). The diffusion dynamics of both PEGylated cationic and PEGylated anionic nanocarriers in the vitreous has not been reported. To determine diffusion coefficients we used fluorescence correlation spectroscopy (FCS). FCS measures changes in the intensity of emitted light from fluorophores and fluorophore labeled/containing species (e.g. nanocarriers, proteins etc.)

across a fixed focal volume, resulting in data as a pulse sequence (Elson and Magde, 1974; Hess et al., 2002; Kristensen et al., 2016; Magde et al., 1974). Autocorrelation analysis of the pulse lag-time provides information about the diffusive speed of the fluorescent species. All previous studies on nanocarrier diffusion in the vitreous that we are aware of have utilized particle tracking (Xu et al., 2013; Martens et al., 2013; Käsdorf et al., 2015), which has distinct advantages (particularly around particle flight dynamics) but is not a bulk system measurement (i.e. reflective of thousands of carriers). FCS of fluorescent nanocarriers allows the diffusion coefficient of a system to be determined from thousands of nanocarriers in crowded media. Furthermore, through cross-correlation of autocorrelation differences between different fluorophores in the nanocarrier we can eliminate any uncertainty associated with fluorophore leakage (if the fluorophore is not covalently bound to the carrier) and potential chemical reactions between a fluorophore and environmental components. Additionally most previous reports on nanocarrier diffusion in the vitreous have used the bovine vitreous as a model. Literature however suggest that the porcine vitreous, in terms of structure and visco-elastic properties, is a better model for the human vitreous (Swindle et al., 2008) and is why the porcine eye is chosen as a model in this study.

Here we use a modified Miyake-Apple technique to introduce a window into the vitreous of an *ex vivo* porcine eye (see Figure 1) and for the first time determine the diffusion coefficients of PEGylated liposomes in the intact vitreous using FCS. We compare these values to diffusion coefficients of PEGylated liposomes in HEPES saline buffer. We show the biodistribution of PEGylated liposomes in the *ex vivo* porcine eye 1 hour after intravitreal injection and discuss this data in light of the determined diffusion coefficients in the vitreous.

2. Materials and methods

2.1 Materials

Cholesterol (Chol), 1,2-distearoyl-3-trimethylammonium-propane (DSTAP), 1,2-distearoyl-sn-glycero-3-phosphocholine (DSPC), 1,2-distearoyl-sn-glycero-3-phosphoethanolamine-N-methoxy(polyethylene glycol)-2000 (DSPE-2000) and 1,2-dipalmitoyl-sn-glycero-3-phosphoethanolamine-N-lissamine rhodamine B (DPPE-Rhod) were all purchased for Avanti Polar Lipids (Alabama, USA), all lipids was >98-99% pure. Calcein (purity >93%), HEPES (purity >99.5%) and NaCl (99%) were all purchased from SigmaAldrich (Brønby, Denmark). FluoSpheres (25 nm and 47 nm) and M-1 embedding matrix and were purchased from ThermoFisher (Paisley, UK). Porcine eyes (Danish Landrace pigs) were obtained from local abattoirs within 2 hours of slaughter.

2.2 Methods

2.2.1 Liposome preparation: The 3 liposome systems were prepared by hydrating dry lipid films with a 10 mM calcein (SigmaAldrich) in 10 mM HEPES saline buffer (pH 7.4, 150 mM NaCl) followed by extrusion through a 100 nm filter at 75 °C (Andresen et al., 2004). Non-encapsulated calcein was removed by size exclusion chromatography on a Sephadex G-50 column using a 10 mM HEPES saline eluent. The anionic system comprised of DSPC, Chol, DSPE-PEG2000 and DPPE-Rhod (54.8:40:5:0.2 mol%) whilst the neutral and cationic systems comprised of DSPC, DSTAP, Chol, DSPE-PEG2000 and DPPE-RhoB (44.8:10:40:5:0.2 and 24.8:30:40:5:0.2 mol% respectively).

2.2.2 Liposome characterisation: The hydrodynamic diameter and surface charge of the liposomes were measured on a Brookhaven ZetaPALS, Zeta potential analyzer. Diameters were measured by dynamic light scattering (DLS) in 10 mM HEPES saline buffer whilst zeta potentials were measured in 10 mM HEPES in 5% glucose solution. Phospholipid concentrations were determined by quantifying the phosphorous content in the purified liposomes samples using ICP-MS.

2.2.3 FCS: Porcine eyes were obtained from a local abattoir, kept on ice and used within 2 hours of slaughter. Excess connective tissue was removed from the eyes. A Miyake-Apple window was introduced into the vitreous by removing part of the sclera and mounting a chamber slide using super glue (Davis et al., 2004; Pereira et al., 2009). This setup enabled optical access to the vitreous while preserving vitreous fine structure. Eyes were injected with 100 µL of a 1 mM liposome suspension in 10 mM HEPES saline buffer (pH 7.4 approximately 5 mm posterior to the corneal limbus at a depth of approximately 0.8 using a 27G needle (Mains et al., 2011)). The porcine eye was not perfused to eliminate convection and active transport factors. A low concentration of liposomes was used to eliminate hydrostatic and osmotic effects between liposomes (Brady, 1993). Control experiments with liposomes in HEPES saline was preformed in 8 chamber slides in a total volume of 500 µL, per well.

FCS was performed on a custom-built fluorescence microscope using 2 photon excitation as previously described in (Brewer et al., 2010; Kubiak et al., 2011). FCS data was analysed using the software SimFCS (Beechem and Gratton, 1988). A laser wavelength of 894 nm, a sampling frequency of 20 kHz and a 60x 1.2 NA water emersion objective were used. Measurements were taken in the central vitreous (Sebag, 1992), at least 100 µm from the cover glass thereby eliminating edge effects. The size of the focal volume was determined by calibrating the system with FluoSpheres (Thermofisher, Ø 25 nm and 47 nm) in buffer and fitting with the locked diffusion coefficients (17.2 $\mu m^2 s^{-1}$ and 9.1 $\mu m^2 s^{-1}$ respectively) determined by the Stokes-Einstein equation assuming temperature to be 293 K and the dynamic viscosity of water to be 1 cP. The focal waist, at 1/e, was found to be 459 nm for the 894 nm laser (global χ^2 <0.01) and, using 2-photon formulas (Krichevsky and Bonnet, 2002). This corresponds to a two photon beam waist of 324 nm and the focal volume was calculated to be 0.8 μm^3. Control experiments of liposome diffusion were made in 10mM HEPES saline

buffer (pH 7.4). Data files were analyzed in sets of 16k points, using the large vector correlation (SimFCS). Data sets that deviated from the autocorrelation function in shape, e.g. showed bumps that could be attributed to noise related events, were deleted. The resulting correlation average files (approx. 10 per set) were then fitted as described in (Brewer et al., 2010) to find the bulk diffusion constant of the liposomes (see Figure 2).

2.2.4 Liposome biodistribution: Porcine eyes were obtained and injected as described in the FCS methodology. After injection, porcine eyes were kept static and moist at room temperature for 1 hour before snap freezing at $-179°C$ in an isopentane/liquid nitrogen bath to minimize water crystal size. The eyes were embedded in M-1 embedding matrix before cryo-sectioning into 40 μm thick sections at 500 μm intervals moving from the lens to the retina. To simplify the biodistribution, the vitreous was divided into 4 segments (1-4), moving from the back of the lens (1) to the vitreoretinal interface (4), with each segment comprising of 4 tissue sections (each section was approx. 1.5 cm^2). Images of sections were captured with confocal microscopy over the whole cross-section of the vitreous cavity. The red fluorescence signal (associated with DPPE-Rhod) in each image was quantified using ImageJ software. To eliminate possible noise contributions, only pixels with an intensity ≥ 50 arbitrary units were counted. Counts were then averaged for all images within each section, before normalizing to the total pixel count of each eye. Red fluorescence was chosen to improve signal to noise intensity whilst removing contributions from collagen auto-fluorescence.

3. Results and discussion

3.1 Liposome characterization and diffusion

Liposomes with similar sizes and size polydispersity but different surface charges were prepared (see Table 1). We chose a zeta potential for the anionic system to be within physiological range (eukaryotic cell membrane zeta potentials range usually within -15 to -30

mV (Alqawlaq et al., 2014; Giannaccini et al., 2014; Koo et al., 2012; Liu et al., 2011; Peeters et al., 2005)) and for the cationic system a relatively low zeta potential. Cationic nanocarriers with significantly high positive zeta potentials as well as liposomes with large concentrations of DSTAP have both been shown to be significantly cytotoxic (Aramaki et al., 1999; Filion and Phillips, 1997; Nel et al., 2009). The PEG composition was kept at 5 mol% to ensure a brush PEG configuration (Garbuzenko et al., 2005).

FCS autocorrelation curves for all systems, whether in buffer or vitreous, could be fitted assuming normal rather than abnormal diffusion. Figure 3 shows the diffusion coefficients of the liposome systems in buffer and in porcine vitreous. Good cross-correlation between the red and green detector channels in the FCS (associated with calcein and DPPE-RhoB respectively in the liposome aqueous core and membrane) was observed. This indicated that neither fluorophore leaked from the liposomes and that liposomes diffused intact through both buffer and vitreous. The average of the apparent diffusion coefficients of the liposome systems, as determined from the red and green detector channels, in HEPES saline buffer (D_{Buff}) were 5.36, 4.82 and 5.11 $\mu m^2 s^{-1}$ for the anionic, neutral and cationic systems respectively. In HEPES saline buffer all liposomes showed similar diffusion coefficients and no significant difference (one-way ANOVA p>0.66). The FCS determined diameters of the liposomes (data not shown) were similar but slightly smaller than those determined by DLS. Nanocarrier diameters determined by FCS and DLS do not always correlate due to a range of factors, including laser induced localized temperature effects, assumptions over medium dynamic viscosity etc. (Drabik et al., 2016; Khan et al., 2016). However, both techniques indicated that no significant liposome agglomeration occurred, even at physiological salt concentrations (i.e. 150 mM) (Stylianopoulos et al., 2010) where repulsive potential energy components (e.g. electrostatic repulsion) become negligible compared to low/no salt solutions. In the vitreous all liposome systems showed reduced diffusion coefficients (see

Figure 3B). The average apparent diffusion coefficients (D_{Vit}) were 2.87, 2.78 and 1.14 $\mu m^2 s^{-1}$ for the anionic, neutral and cationic systems respectively. Comparing the effective diffusion in the vitreous between the different liposome systems it can be seen that the cationic liposomes diffuse slower than the anionic and neutral liposomes ($p<0.01$). This indicates that the observed reduction of the diffusion coefficients cannot solely be explained by the increased dynamic viscosity of the vitreous compared to saline buffer.

For the neutral system, the ratio of buffer diffusion coefficient to vitreous diffusion coefficient (i.e. $D_{Buff}/D_{Vit.}$, see Figure 4) was 1.73 and in general agreement with previously reported ratios (between 1.8-3.2) for PEGylated polymeric nanoparticles in the bovine vitreous. These polymeric nanoparticles had diameters from 100 to 200 nm and zeta potentials between -4 to -8 mV (Käsdorf et al., 2015; Martens et al., 2013; Peeters et al., 2005; Xu et al., 2013). Surprisingly, the $D_{Buff}/D_{Vit.}$ ratio of the anionic liposome system (i.e. 1.87) is lower than reported values (between 2.2-3.2) for carboxylic acid functionalized anionic polymeric nanoparticles (Martens et al., 2013; Xu et al., 2013). These -COOH functionalized polymeric nanoparticles had zeta potentials ranging from -49 to -65 mV and diameters between 100 to 200 nm. The observed lower $D_{Buff}/D_{Vit.}$ ratio for the anionic liposome system likely reflects a range of factors. These include physiological factors associated with intraspecies and interspecies (bovine eye studies dominate the literature) variations in CGN density, as well as differences in the physicochemical properties of nanocarrier systems. In fact literature suggests that the porcine vitreous has a lower loss modulus, hence a lower dynamic viscosity than the bovine vitreous (Filas et al., 2014; Nickerson et al., 2008). However the large variability on the viscosity measurements within each species prohibits quantification of the expected difference in D_{Vit} between porcine and bovine. Additionally liposomes are highly deformable compared to rigid solid polymeric nanoparticles and this flexibility may facilitate diffusion through CGN pores, particularly pores with sizes that approach that of the

nanocarrier. These factors together are a possible explanation for the slightly lower D_{Buff}/D_{Vit} observed for neutral and negative liposomes compare to what has previously been reported (Käsdorf et al., 2015; Martens et al., 2013; Xu et al., 2013).

The cationic liposome system showed the greatest decrease in diffusion coefficient moving from buffer to vitreous and the largest $D_{Buff}/D_{Vit.}$ ratio (i.e. 4.48). Xu et al. reported a D_{Water}/D_{Vit} ratio of 2200 for amine functionalized polystyrene nanoparticles (Ø = 181 nm, +39 mV zeta potential) (Xu. et al., 2013) whilst for a similar amine functionalized polystyrene system (Ø = 107 nm, +39 mV zeta potential) Martens et al. reported a $D_{Buff}/D_{Vit.}$ ratio of 13 (Martens et al., 2013). Both groups reported that the cationic polymeric nanoparticles did not significantly diffuse away from the injection site. If we had observed similar values for the cationic liposome system we would have obtained D_{Vit} values between 2.2×10^{-3} and 0.37 $\mu m^2 s^{-1}$. There are a number of challenges with directly comparing data between the systems. Similar to the anionic systems, there are both differences in physiology and material properties. These previous studies used bovine vitreous, which has a higher viscosity than the porcine vitreous (Filas et al., 2014; Nickerson et al., 2008). The difference in viscosity could explain the lower D_{Vit} reported by Martens et al. but not the D_{Vit} reported by Xu et. al. The difference in zeta potential between the cationic liposomes and the cationic polymeric nanoparticles is an additional significant difference (i.e. +11.9 mV versus +39 mV). The CGN is viewed as having a net negative charge and it would be easy to argue that large cationic charge increases electrostatic attraction between nanocarrier and the CGN, resulting in little or no diffusion. As the surface charge drops, the likelihood of strong electrostatic attraction diminishes and nanocarrier diffusion increases through the CGN. If we assume that the porcine vitreous has a similar sodium salt concentration to human vitreous (i.e. approximately 150 mM) (Kokavec et al., 2016), then the Debye screening length for the vitreous would be approximately 0.7 nm (Freudenberg et al., 2007). This reduced screening length would promote attractive

interactions between nanocarriers with high surface energies whilst substantially reducing electrostatic repulsion, leading to nanocarrier agglomeration (i.e. a reduction of the system potential energy). Our systems showed no agglomeration in buffer with salt concentrations similar to the vitreous. Other reported studies measure particle size in either pure water or low salt concentrations (e.g. 10 mM) which greatly increases the Debye screening length and therefore maximizes electrostatic repulsion between nanocarriers. This opens the question as to whether previous observations regarding limited mobility or immobilized cationic non-PEGylated nanocarriers are a result of nanocarrier agglomeration rather than nanocarrier-CGN interactions. Agglomerated nanocarriers (even if agglomerates contain only a small number of nanocarriers) would increases particulate size resulting in inhibited diffusion through CGN pores rather than reducing diffusion through electrostatic attraction.

All the liposomes systems contain 5 mol% DSPE-PEG2000, which ensures that surface PEG is in a brush configuration (Garbuzenko et al., 2005) and therefore long circulating. It has been calculated that the brush configuration of PEG extends approximately 4.5 nm from the liposome surface (mushroom configuration extends 3.3 nm) (Garbuzenko et al., 2005). It would not be unreasonable to assume that PEG chains (either in brush or mushroom configuration) would sterically inhibit the distance of approach between liposome and CGN, thereby reducing electrostatic interactions. As the liposomes are in the liquid ordered phase and have a high cholesterol content (40 mol%), it also seems unlikely that DSPE-PEG2000 phospholipids could be easily displaced to allow the liposome to approach the CGN to within ≤ 1 nm. Furthermore, studies on PEGylated polymeric nanoparticles have shown that PEGylation eliminates any bound fraction of nanoparticles in the vitreous, indicating that PEG chains inhibit nanoparticle-CGN interactions (Käsdorf et al., 2015). Our results show that, even with brush configuration PEG surface densities that should inhibit nanoparticle-CGN interactions and shield electrostatic interactions, weak electrostatic interactions occurred

between the cationic system and the CGN. The argument for weak interactions over strong interactions is supported by the observed diffusion of cationic liposomes in the vitreous. As there appears to be weak electrostatic attraction between the cationic system and the CGN, it could be that there is a weak electrostatic repulsion between the anionic system and the CGN. This repulsion in combination with PEGylation could account for the lower $D_{Buff}/D_{Vit.}$ ratio observed for the anionic liposomes compared to anionic polymer systems.

There are a number of possible physiological explanations for the observation regarding cationic liposomes. It may be that the porcine eyes used for the cationic liposomes had lower CGN densities compared with bovine eyes, minimizing nanocarrier-CGN interactions and decreasing vitreous viscosity. This could also possibly explain why the anionic liposomes had a lower D_{Buff}/D_{Vit} ratio than anionic polymeric nanoparticles in the bovine vitreous. It may be that porcine vitreous has a higher salt concentration than bovine vitreous. The bovine vitreous would therefore have a longer Debye screening length causing increased electrostatic interactions between nanocarrier and the CGN. It may be that salt concentrations within the vitreous are not uniform and that at the submicron scale there may be regions of lower salt concentration which would greatly increase the Debye screening length and therefore overcome the steric factor associated with PEG chains. Combined with these low salt regions could be high CGN density regions with small pores, which would also increase the probability of electrostatic interactions. These final two explanations are undermined by the lack of any observed anomalous diffusion in the autocorrelation curves as it could be envisaged that anomalous diffusion (e.g. Lévy flight and trap dynamics) would occur if the vitreous had submicron regions with substantial variations in physicochemical properties.

3.2 Liposome distribution in the eye

The biodistribution of the liposomes was tested to determine whether liposome surface chemistry and corresponding diffusion coefficient influenced distribution dynamics in the porcine eye (see Figure 5). To aid analysis and presentation, the vitreous was divided into 4 segments (1-4), moving from the lens (1) to the vitreoretinal interface (4). Figure 6 shows the biodistribution data and the median and interquartile range for the liposome systems. Mean values were avoided to eliminate large values outweighing small values in normalized fluorescence. Taking the median values across the 4 segments for both the anionic (Figure 6A) and neutral systems (Figure 6B), it can be seen that there is a relatively even distribution for both sets of liposomes (0.15-0.32 for the anionic and 0.16-0.27 for the neutral). One hour post injection the cationic system (Figure 6C) showed an uneven distribution with the largest median values (0.32 and 0.4) located in the middle segments of the vitreous. The cationic system also showed the lowest median value for the front of the vitreous (0.05), one hour after injection, compared with the other two systems. As the intravitreal injection occurred approximately 5mm from the corneal limbus (at the segment 1 and 2 interface) the elevated levels in the middle of the vitreous might reflect a combination of slower diffusion and convection currents associated with injection. To determine if this might be the case, we repeated the biodistribution study of the cationic system but snap-froze the eyes after 2 hours to account for the slower diffusion rate (see Figure 6D). It could be seen that after 2 hours both the median values for segments 1 and 4 (front and back vitreous) had increased to 0.16 and 0.25, whilst the median values of the middle vitreous had decreased.

Overall, there is little substantial difference in distribution between the liposome systems. We observed no significant compartmentalization of liposomes into specific segments (e.g. remaining at the injection site, preferential diffusion to the vitreoretinal region etc.) under passive diffusion conditions. This indicates that PEGylation eliminated any bound fractions of liposomes as previously shown with polymeric nanocarriers (Käsdorf et al., 2015; Xu et al.,

2016). Furthermore, the weak electrostatic interactions observed had no apparent effect on the distribution of the liposomes. Although the low diffusion rate of the cationic system did influence short-term biodistribution, this distribution did not remain with extended time.

4. Conclusions

Our work demonstrates that PEGylated cationic liposomes can diffuse through the vitreous and can reach the vitreoretinal region. PEGylation did not completely inhibit electrostatic interactions and weak electrostatic attraction is the likely explanation for the reduced diffusion rate of PEGylated cationic liposomes compared to the anionic and neutral systems. High cationic charge in nanocarriers is associated with significant cytotoxicity due to cell membrane disruption. However, it is generally accepted that nanocarriers with cationic surface charge have increased interactions with cell membranes due to electrostatic attraction and a greater likelihood of being endocytosed. Our results show that the combination of PEGylation with cationic surface charge will not inhibit nanocarriers form reaching the vitreoretinal region. This presents a strong argument for combing the benefits of PEGylation and cationic charge in nanocarriers as systems for the treatment of posterior segment diseases. However, many fundamental questions still remain regarding the nature of nanocarrier-CGN dynamics and whether these can be exploited to maximize nanocarrier therapeutic performance.

References:

Alqawlaq, S., Sivak, J., Huzil, T., Ivanova, M., Flanagan, J., Beazely, M., Foldvari, M., 2014. Preclinical development and ocular biodistribution of gemini-DNA nanoparticles after intravitreal and topical administration: towards non-invasive glaucoma gene therapy. Nanomedicine : nanotechnology, biology, and medicine 10, 1637–47.

Andresen, T.L., Davidsen, J., Begtrup, M., Mouritsen, O.G., Jørgensen, K., 2004. Enzymatic

release of antitumor ether lipids by specific phospholipase A2 activation of liposome-forming prodrugs. J. Med. Chem. 47, 1694–703.

Aramaki, Y, Takano, S, Tsuchiya, S, 1999. Induction of apoptosis in macrophages by cationic liposomes. FEBS letters, 460(3), 472-476.

Beechem, J., Gratton, E., 1988. Fluorescence Spectroscopy Data Analysis Environment: A Second Generation Global Analysis Program 70–81.

Bochot, A., Fattal, E., 2012. Liposomes for intravitreal drug delivery: A state of the art. Journal of Controlled Release, 161(2), 628-634.

Brady, J.F., 1993. Brownian motion, hydrodynamics, and the osmotic pressure. The Journal of chemical physics 98, 3335–3341.

Brewer, J, Serna, JB de la, Wagner, K, 2010. Multiphoton excitation fluorescence microscopy in planar membrane systems. Biochimica et Biophysica Acta (BBA)-Biomembranes, 1798(7), 1301-1308.

Congdon, NG, Friedman, DS, Lietman, T, 2003. Important causes of visual impairment in the world today. Jama, 290(15), 2057-2060.

Davis, B., Nilson, C., Mamalis, N., 2004. Revised Miyake–Apple technique for postmortem eye preparation. Journal of Cataract & Refractive Surgery 30, 546549.

Drabik, D, Przybyło, M, Sikorski, A, Langner, M, 2016. The Effect of a Fluorophore Photo-Physics on the Lipid Vesicle Diffusion Coefficient Studied by Fluorescence Correlation Spectroscopy. Journal of fluorescence, 26(2), 661-669.

Elson, Magde, 1974. Fluorescence correlation spectroscopy. I. Conceptual basis and theory. Biopolymers, 13(1), 1-27.

Filas, B., Zhang, Q., Okamoto, R., Shui, Y.-B., Beebe, D., 2014. Enzymatic Degradation Identifies Components Responsible for the Structural Properties of the Vitreous BodyStiffness and Adhesivity of the Vitreous. Investigative Ophthalmol Vis Sci 55, 55–63.

Filion, MC, Phillips, NC, 1997. Toxicity and immunomodulatory activity of liposomal vectors

formulated with cationic lipids toward immune effector cells. Biochimica et Biophysica Acta (BBA) -Biomembranes, 1329(2), 345-356.

Foulds, WS, 1987. Is your vitreous really necessary? Eye, 1(6), 641-664.

Freudenberg, U, Behrens, SH, Welzel, PB, Müller, M, 2007. Electrostatic interactions modulate the conformation of collagen I. Biophysical journal, 92(6), 2108-2119.

Garbuzenko, O, Barenholz, Y, Priev, A, 2005. Effect of grafted PEG on liposome size and on compressibility and packing of lipid bilayer. Chemistry and physics of lipids, 135(2), 117-129.

Geng, S., Yang, B., Wang, G., Qin, G., Wada, S., Wang, J.-Y., 2014. Two cholesterol derivative-based PEGylated liposomes as drug delivery system, study on pharmacokinetics and drug delivery to retina. Nanotechnology 25, 275103.

Giannaccini, M., Giannini, M., Calatayud, Goya, G., Cuschieri, A., Dente, L., Raffa, V., 2014. Magnetic Nanoparticles as Intraocular Drug Delivery System to Target Retinal Pigmented Epithelium (RPE). International Journal of Molecular Sciences 15(1), 1590-1605.

Goff, M.M. Le, Bishop, P.N., 2008. Adult vitreous structure and postnatal changes. Eye (Lond) 22, 1214–22.

Hess, ST, Huang, S, Heikal, AA, Webb, WW, 2002. Biological and chemical applications of fluorescence correlation spectroscopy: a review. Biochemistry, 41(3), 697-705.

Holekamp, NM, 2010. The vitreous gel: more than meets the eye. American journal of ophthalmology, 149(1), 32-36.

Holekamp, N.M., Shui, Y.-B.B., Beebe, D.C., 2005. Vitrectomy surgery increases oxygen exposure to the lens: a possible mechanism for nuclear cataract formation. Am. J. Ophthalmol. 139, 302–10.

Käsdorf, BT, Arends, F, Lieleg, O, 2015. Diffusion Regulation in the Vitreous Humor. Biophysical journal, 109(10), 2171-2181.

Khan, M., Singh, M., Sen, S., 2016. Measuring Size, Size Distribution, and Polydispersity of Water-in-Oil Microemulsion Droplets using Fluorescence Correlation Spectroscopy:

Comparison to Dynamic Light Scattering. The Journal of Physical Chemistry B 120, 1008–1020.

Kodama, M, Matsuura, T, Hara, Y, 2013. Structure of vitreous body and its relationship with liquefaction.

Kokavec, J, Min, SH, Tan, MH, Gilhotra, JS, 2016. Biochemical analysis of the living human vitreous. Clinical & experimental ophthalmology, 44(7), 597-609.

Koo, H., Moon, H., Han, H., Na, J., Huh, M., Park, J., Woo, S., Park, K., Kwon, I., Kim, K., Kim, H., 2012. The movement of self-assembled amphiphilic polymeric nanoparticles in the vitreous and retina after intravitreal injection. Biomaterials 33, 34853493.

Krichevsky, O., Bonnet, G., 2002. Fluorescence correlation spectroscopy: the technique and its applications. Reports on Progress in Physics 65, 251.

Kristensen, K., Urquhart, A.J., Thormann, E., Andresen, T.L., 2016. Binding of human serum albumin to PEGylated liposomes: insights into binding numbers and dynamics by fluorescence correlation spectroscopy. Nanoscale 8, 19726–19736.

Kubiak, J, Brewer, J, Hansen, S, Bagatolli, LA, 2011. Lipid lateral organization on giant unilamellar vesicles containing lipopolysaccharides. Biophysical journal, 100(4), 978-986.

Li, H, Palamoor, M, Jablonski, MM, 2016. Poly (ortho ester) nanoparticles targeted for chronic intraocular diseases: ocular safety and localization after intravitreal injection. Nanotoxicology, 10(8), 1152-1159.

Liu, H., Liu, Y., Ma, Z., Wang, J., Zhang, Q., 2011. A lipid nanoparticle system improves siRNA efficacy in RPE cells and a laser-induced murine CNV model. Investigative ophthalmology & visual science 52, 4789–94.

Liu, S., Jones, L., Gu, F., 2012. Nanomaterials for Ocular Drug Delivery. Macromolecular Bioscience, 12(5), 608-620.

Magde, D, Elson, EL, Webb, WW, 1974. Fluorescence correlation spectroscopy. II. An experimental realization. Biopolymers, 13(1), 29-61.

Mains, J., Wilson, C., 2013. The Vitreous Humor As a Barrier to Nanoparticle Distribution. Journal of Ocular Pharmacology and Therapeutics 29, 143150.

Mains, J., Wilson, C., Urquhart, A., 2011. ToF-SIMS analysis of ocular tissues reveals biochemical differentiation and drug distribution. European Journal of Pharmaceutics and Biopharmaceutics 79, 328333.

Martens, T., Vercauteren, D., Forier, K., Deschout, H., Remaut, K., Paesen, R., Ameloot, M., Engbersen, J., Demeester, J., Smedt, S., Braeckmans, K., 2013. Measuring the intravitreal mobility of nanomedicines with single-particle tracking microscopy. Nanomedicine, 8(12), 1955-1968.

Natarajan, J.V., Darwitan, A., Barathi, V.A., Ang, M., Htoon, H.M., Boey, F., Tam, K.C., Wong, T.T., Venkatraman, S.S., 2014. Sustained drug release in nanomedicine: a long-acting nanocarrier-based formulation for glaucoma. ACS Nano 8, 419–29.

Nel, A., Mädler, L., Velegol, D., Xia, T., Hoek, E., Somasundaran, P., Klaessig, F., Castranova, V., Thompson, M., 2009. Understanding biophysicochemical interactions at the nano-bio interface. Nat Mater 8, 543–57.

Nickerson, C., Park, J., Kornfield, J., Karageozian, H., 2008. Rheological properties of the vitreous and the role of hyaluronic acid. J Biomech 41, 1840–1846.

Peeters, L., Sanders, N. N., Braeckmans, K., Boussery, K., Van de Voorde, J., De Smedt, S. C., & Demeester, J. (2005). Vitreous: a barrier to nonviral ocular gene therapy. Investigative ophthalmology & visual science, 46(10), 3553-3561.

Pereira, F., Werner, L., Milverton, J., Coroneo, M., 2009. Miyake-Apple posterior video analysis/photographic technique. Journal of cataract and refractive surgery 35, 577–87.

Pozo-Rodríguez, A. del, Delgado, D., Gascón, A., Solinís, M., 2013. Lipid Nanoparticles as Drug/Gene Delivery Systems to the Retina. Journal of Ocular Pharmacology and Therapeutics, 29(2), 173-188.

Sakurai, E., Ozeki, H., Kunou, N., Ogura, Y., 2001. Effect of particle size of polymeric

nanospheres on intravitreal kinetics. Ophthalmic Res. 33, 31–6.

Scott, JE, 1992. The chemical morphology of the vitreous. Eye, 6(6), 553-555.

Sebag, J, 1992. Anatomy and pathology of the vitreo-retinal interface. Eye, 6(6), 541-552.

Sebag, J, 2009. Vitreous: the resplendent enigma. British Journal of Ophthalmology, 989-991.

Stefansson, E, Loftsson, T, 2006. The Stokes– Einstein equation and the physiological effects of vitreous surgery. Acta Ophthalmologica Scandinavica, 84(6), 718-719.

Stylianopoulos, T, Poh, MZ, Insin, N, Bawendi, MG, 2010. Diffusion of particles in the extracellular matrix: the effect of repulsive electrostatic interactions. Biophysical journal, 84(6), 718-719.

Thakur, S.S., Barnett, N.L., Donaldson, M.J., Parekh, H.S., 2014. Intravitreal drug delivery in retinal disease: are we out of our depth? Expert opinion on drug delivery, 11(10), 1575-1590.

Xu, X, Xu, Z, Liu, J, Zhang, Z, Chen, H, Li, X, 2016. Visual tracing of diffusion and biodistribution for amphiphilic cationic nanoparticles using photoacoustic imaging after ex vivo intravitreal injections. International journal of nanomedicine, 11, 5079.

Xu, Q., Boylan, N., Suk, J., Wang, Y.-Y., Nance, E., Yang, J.-C., McDonnell, P., Cone, R., Duh, E., Hanes, J., 2013. Nanoparticle diffusion in, and microrheology of, the bovine vitreous ex vivo. Journal of Controlled Release, 167(1), 76-84.

Yau, G., Almeida, D.R., Chin, E.K., Park, S.S., 2015. Age-related macular degeneration. Handbook of Vitreo-Retinal Disorder Management: A Practical Reference Guide 33.

Yau, J., Rogers, S., Kawasaki, R., Lamoureux, E., Kowalski, J., Bek, T., Chen, S.-J., Dekker, J., Fletcher, A., Grauslund, J., Haffner, S., Hamman, R., Ikram, K., Kayama, T., Klein, B., Klein, R., Krishnaiah, S., Mayurasakorn, K., O'Hare, J., Orchard, T., Porta, M., Rema, M., Roy, M., Sharma, T., Shaw, J., Taylor, H., Tielsch, J., Varma, R., Wang, J., Wang, N., West, S., Xu, L., Yasuda, M., Zhang, X., Mitchell, P., Wong, T., Group, M.-A. for, 2012. Global Prevalence and Major Risk Factors of Diabetic Retinopathy. Diabetes Care 35, 556–64.

Zhao, L., Chen, G., Li, J., Fu, Y., Mavlyutov, T., Yao, A., Nickells, R., Gong, S., Guo, L.-W., 2017. An

intraocular drug delivery system using targeted nanocarriers attenuates retinal ganglion cell

degeneration. J Control Release 247, 153–166.

Figure legends

Figure 1. Schematic diagrams: A) The liposomes comprised of phospholipids, cholesterol, a calcein loaded aqueous core (green), rhodamine (red hexagons) conjugated phospholipids and PEG (black lines) conjugated phospholipids; B) Illustration showing the experimental setup for the *ex vivo* porcine eye used for FCS analysis. A modified Miyake-Apple technique was used to introduce a window into the vitreous (Liposomes shown as red border/green core spheres, whilst the laser light is shown in blue).

Figure 2: Example normalized autocorrelation curves of liposomes in the vitreous of the ex vivo porcine eye. All autocorrelation curves, whether in the vitreous or buffer, could be fitted assuming normal diffusion.

Figure 3. A) The FCS determined diffusion coefficients of liposomes in 10 mM HEPES saline buffer (n = 3 per liposome system); B) The FCS determined diffusion coefficients of liposomes in *ex vivo* porcine vitreous (n = 5 per liposome system). In both figures the diffusion coefficients as determined by the red channel (red column), green channel (green column), cross correlation (gray column) and the average of the combined red and green channels (black columns) are shown. Black error bars show the SEM for each coefficient.

Figure 4. The diffusion coefficient ratios between buffer and vitreous (D_{Buff}/D_{Vit}) for the liposome systems determined from the red channel (red column), green channel (green column), cross correlation (gray column) and the average of the combined red and green channels (black columns) FCS data. Black error bars show the error (as determined by

propagation of the SEM) for each ratio. The average D_{Buff}/D_{Vit} values for the anionic, neutral and cationic systems are 1.87, 1.73 and 4.48 respectively.

Figure 5. An example of a vitreous cross section imaged by confocal microscopy showing red fluorescence (A) and corresponding bright field (B) images. Scale bar corresponds to 40 µm. This image was made with the anionic liposomes. The red fluorescence is associated with DPPE-Rhod.
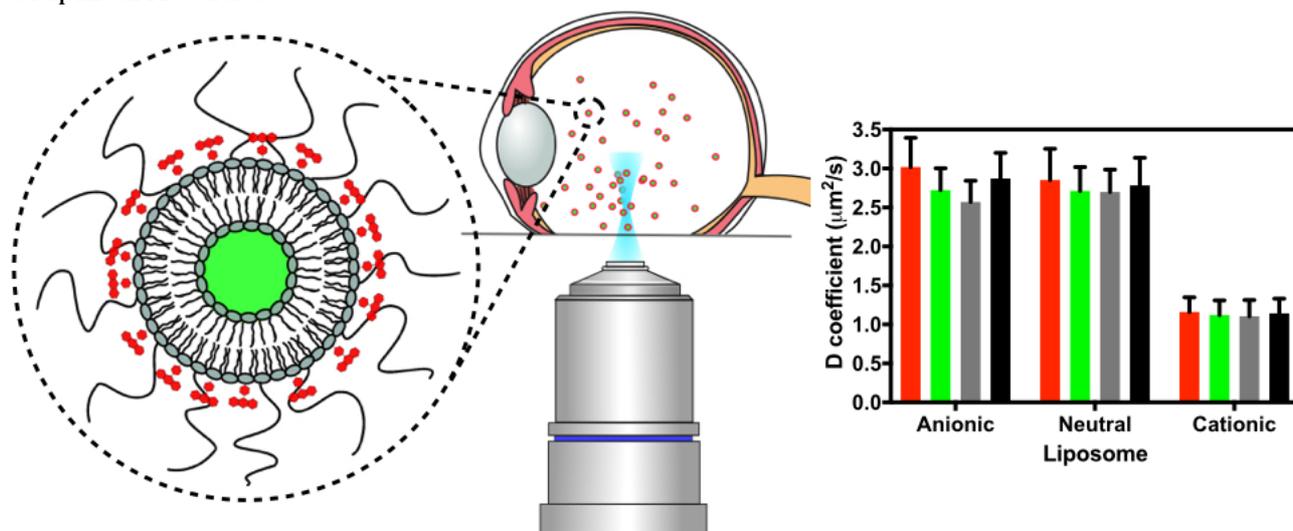
Figure 6. The median and interquartile range of liposome biodistribution after intravitral injection into the *ex vivo* porcine eye. The X axis refers to section in the eye from 1= front vitreous-posterior lens to 4 posterior vitreous-vitreoretinal interface; A) Anionic liposomes 1h post injection B) Neutral liposomes 1h post injection. C) Cationic liposomes 1h post injection. D) cationic liposomes 2h post injection.
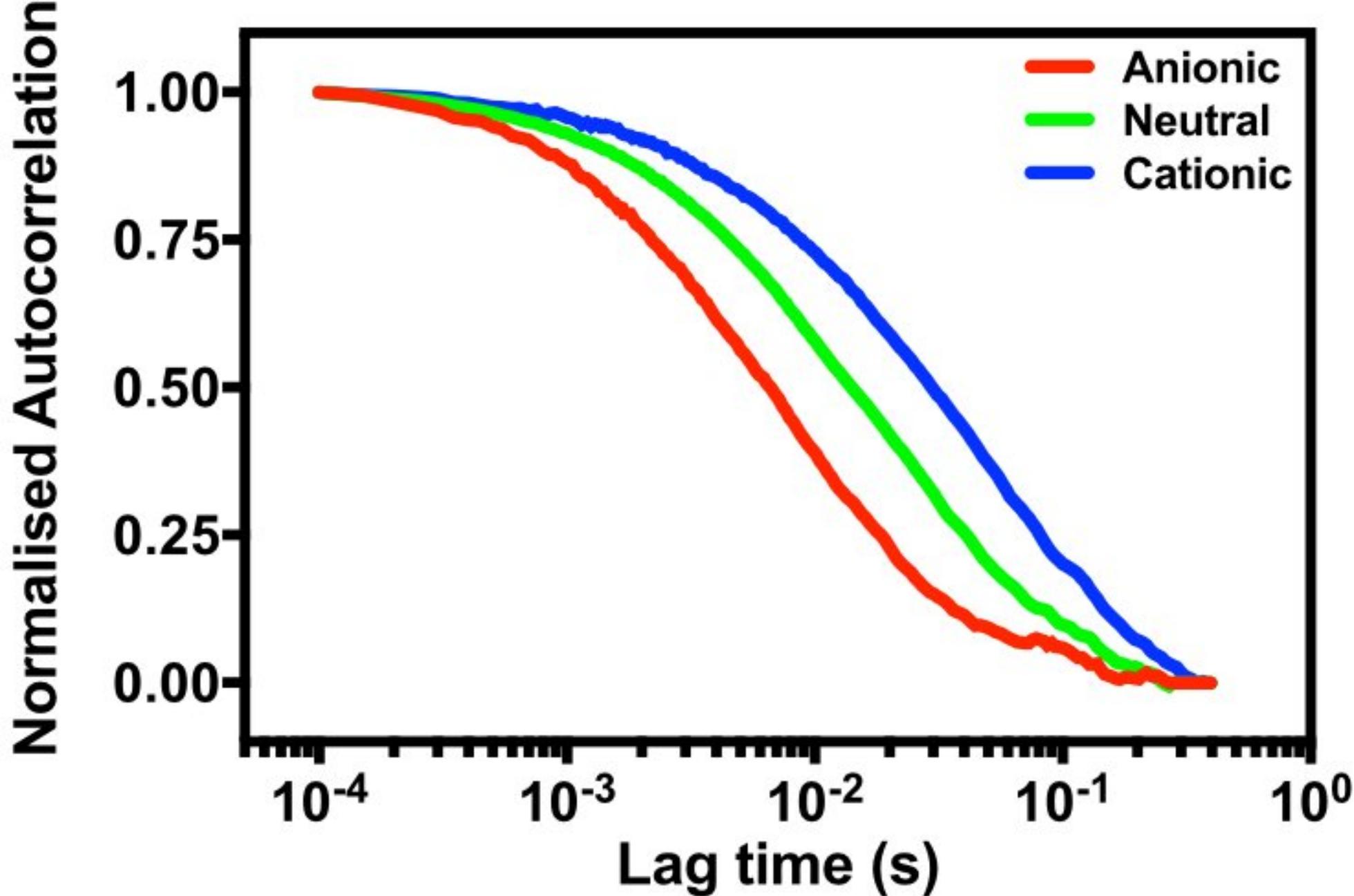
Table and Table legend

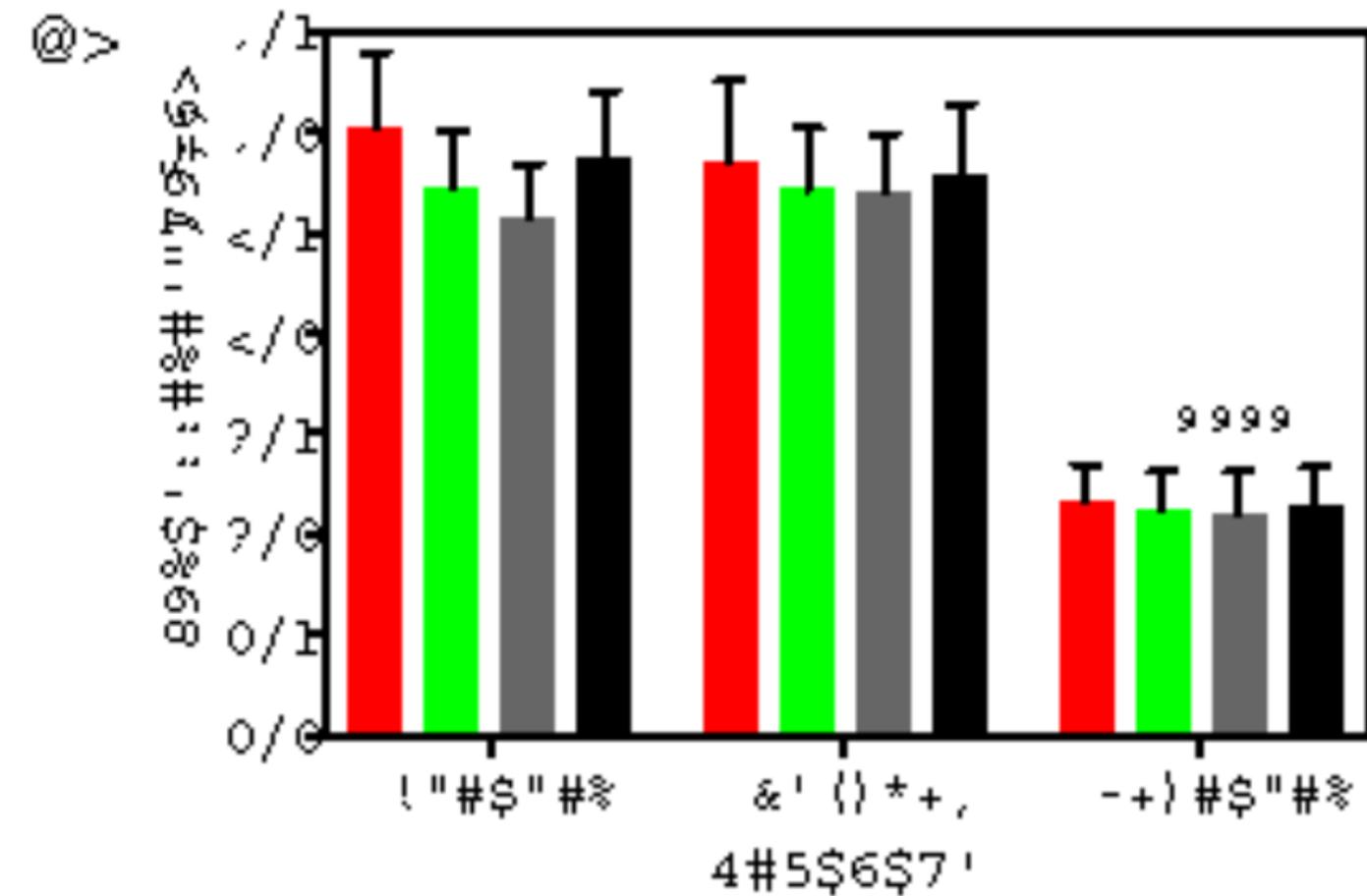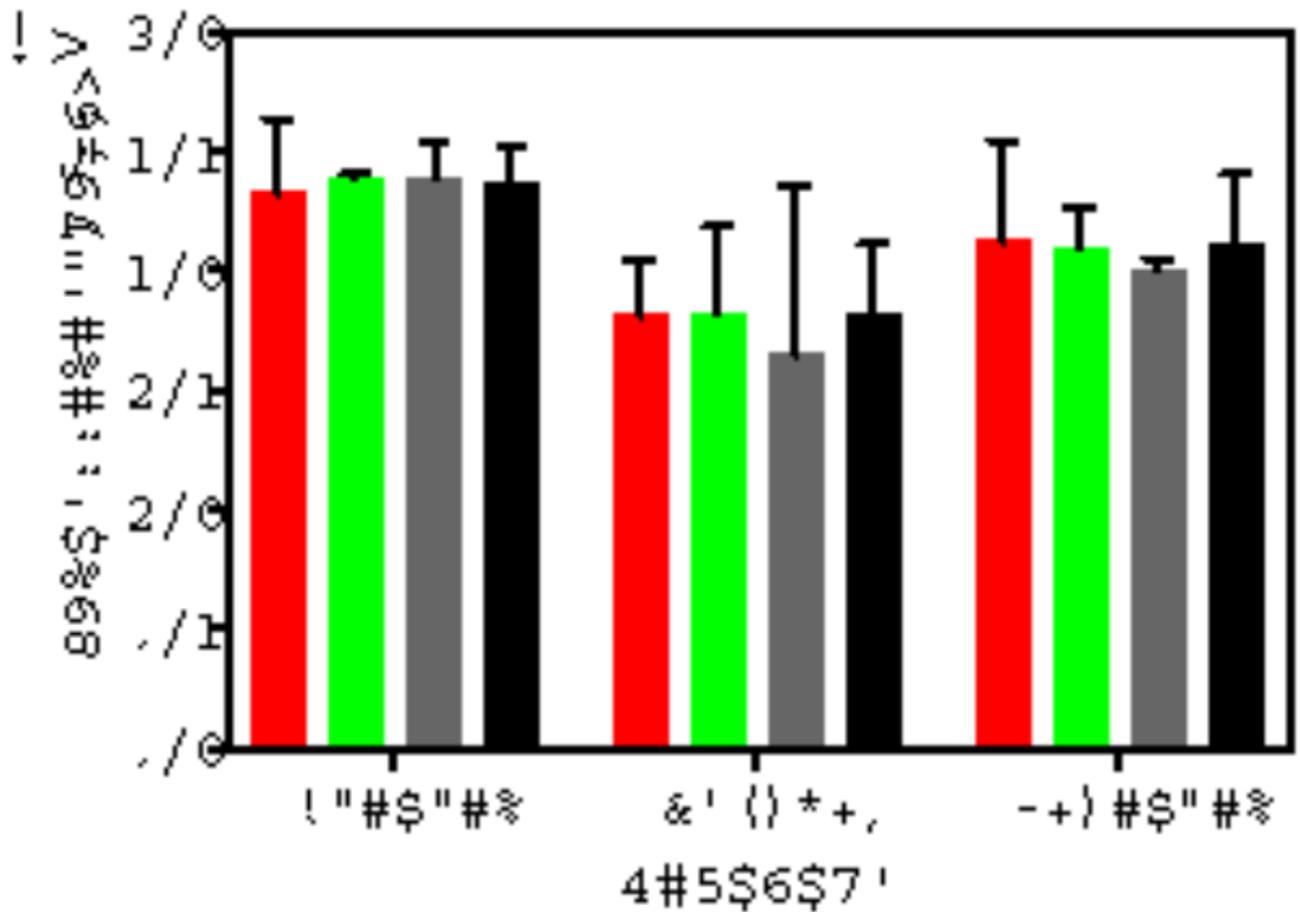| Liposome	Diameter [nm]	PDI	Zeta-potential [mV]
Anionic	121 ±5	0.05 ±0.01	-20.5 ±4
Neutral	135 ±2	0.04 ±0.01	0.0 ±2
Cationic	137 ±5	0.04 ±0.01	11.9 ±2

Table 1. Liposome size and zeta potential. Liposome diameters measured by DLS in 10 mM HEPES saline buffer. Mean ± SEM (n = 5 per liposome system) with the standard error of the mean (SEM). Liposome zeta potential measured in 10mM HEPES 5% Glucose solution. Mean ± SEM (n = 5 per liposome system).
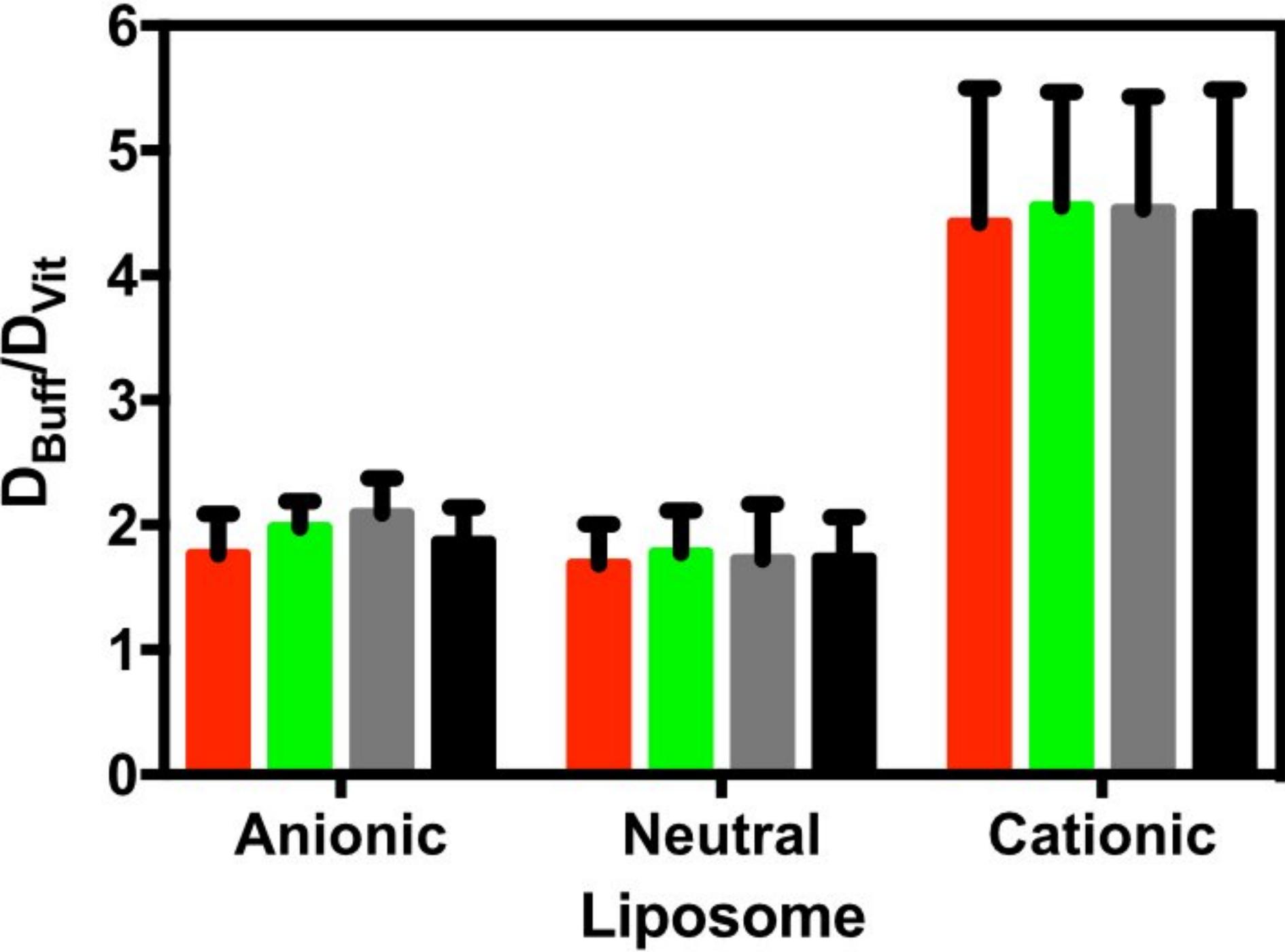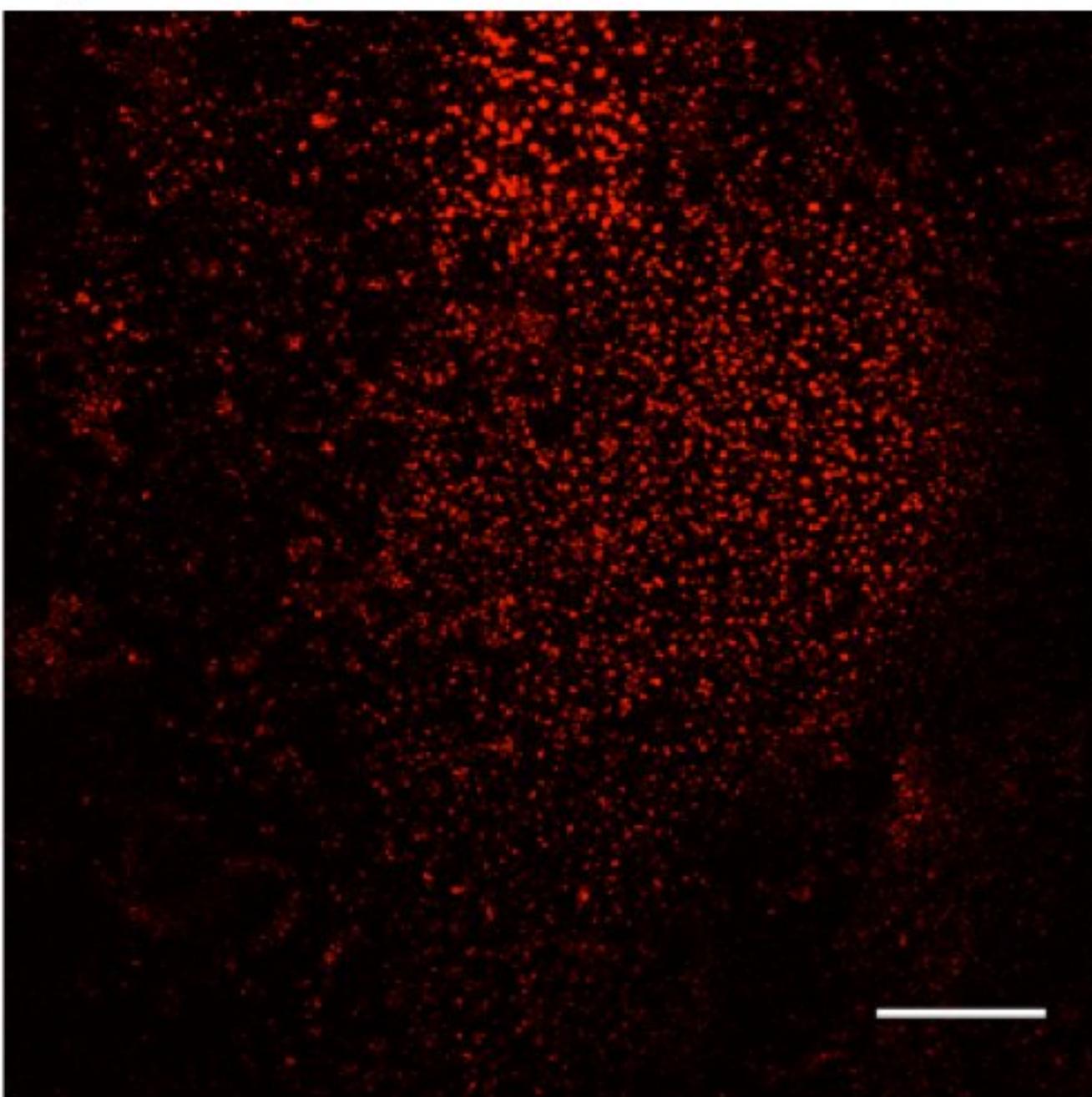
Graphical Abstract